Digital Back Propagation via Sub-band Processing in Spatial Multiplexing Systems

Filipe M. Ferreira, *Senior Member, IEEE*, Eric Sillekens, *Member*, IEEE, Boris Karanov, *Student Member*, IEEE, Robert Killey, *Senior Member, IEEE*

Abstract—An advanced digital backward-propagation (DBP) method using a separate-channels approach (SCA) is investigated for the compensation of inter-channel nonlinearities in spatial- and wavelength-multiplexed systems. Compared to the conventional DBP, intra- and inter-mode cross-phase modulation can be efficiently compensated by including the effect of the inter-channel walk-off in the nonlinear step of the split-step Fourier method. We found that the SCA-DBP relaxes the step size requirements by a factor of 10, while improving performance by 0.8 dB for large walk-off and strong linear coupling. For the first time, it is shown that in spatial multiplexed systems transmission performance can be improved by sub-band processing of back propagated channels.

Index Terms—Digital-Back Propagation, Linear Mode Coupling, Spatial Division Multiplexing.

I. INTRODUCTION

SPATIAL-DIVISION MULTIPLEXING (SDM) has emerged as a very promising solution for overcoming the capacity limit of single-mode fibers (SMFs) [1]. Among the possible SDM approaches, few-mode fibers (FMFs) and coupled-core multi-core (CC-MCFs) offer the highest spatial information density. They exhibit low nonlinear coefficients and high pumping efficiency allowing for high spatial-density integration in transponders [2] and add-drop multiplexers [3]. However, the multitude of spatial modes introduces new impairments, namely: group delay (GD) spread [4-10] stemming from the interplay between differential mode delay (DMD) and linear mode coupling (LMC), inter-mode nonlinear effects (IM-NL) [11-16], and mode dependent loss (MDL) [17-19]. Among these, LMC can play a critical role at reducing the GD spread, MDL accumulation and nonlinear interactions efficiency [20-22]. Thereby, and with practical fibers operating in all LMC regimes [23-30], the modelling of LMC has been under intensive research [4-9] as well as its impact on the statistics of GD, MDL and NL.

The compensation of the linear impairments using digital and analog techniques has been successfully demonstrated for long-haul transmission over 1000s km [31-35]. And more recently, the impact of inter-mode nonlinearities (IM-NL) in SDM systems has been under study [36, 37] – having been shown that their impact is non-negligible. As a consequence, the investigation of applying digital back propagation (DBP) to address the IM-NL penalties in SDM systems has attracted interest [38-41] showing that considerable improvements can be achieved for weak to intermediate linear coupling regime [39] and identifying cases where increasing DBP bandwidth towards full field compensation degrades the performance [41]. In this paper, we explore alternative ways of implementing the nonlinear compensation step in the split-step Fourier method (SSFM) for SDM systems which are characterized by significant decorrelation (as induced by DMD and LMC) between the spatial- and wavelength-division-multiplexed (WDM) channels.

In SDM-WDM systems, the compensation of the four-wave-mixing (FWM) contributions are characteristically complex just like for conventional WDM systems over SMFs [42-45]. The FWM contributions require phase-matching (in contrast to XPM, which is inherently phase-matched). Therefore, the strength of the newly created waves (in the FWM sense) depends on the fiber link DMD and LMC (besides channel spacing, fiber dispersion, signal power, modulation format and baud rate). For instance, for fiber links with weak-to-intermediate LMC, group delay management along the transmission path leads to increased nonlinear efficiency [21] – nevertheless, a relevant scenario since the equalization complexity scales with the group delay spread [10]. Instead, in this manuscript, we focus on systems with strong LMC and non-negligible DMD that are also of major practical relevance since the overall nonlinear efficiency is minimum [46] – FWM efficiency is particularly reduced because of strong phase-mismatching. However, conventional DBP is particularly ill suited for SDM links with significant DMD and strong LMC – similarly to the case of SMF links with unusual large polarization mode dispersion [45]. The reason is that, in conventional DBP, the introduction of FWM products while back-propagating cannot be avoided, even when it is known that during forward propagation the random evolution of the dispersion operator has rendered FWM negligible. The key reason being that conventional DBP considers a single signal envelope representation (per polarization), independently of the number of wavelength channels, preventing a specific type of

F. Ferreira, E. Sillekens, B. Karanov and R. Killey are with the Optical Networks Group, Department of Electronic & Electrical Engineering, University College London, London WC1E 7JE, UK (e-mail: f.ferreira@ucl.ac.uk; e.sillekens@ucl.ac.uk; boris.karanov.16@ucl.ac.uk; r.killey@ucl.ac.uk).

inter-channel nonlinear interaction from being isolated and nulled – note that conventional SMF links with low polarization mode dispersion have no requirement for such feature.

In order to be able to null specific inter-channel nonlinear interactions, signal propagation must be modeled using the separated-channels approach (SCA) [42]. In this approach, the total electric field signal is split into N parallel signals through frequency filtering and frequency down-shifting. In this way, the nonlinear coupling terms corresponding to intra-mode XPM and IM-XPM can be kept while those representing FWM and IM-FWM are nulled. Moreover, while in conventional DBP only one value of the relative position (i.e. walk-off) between the channels is considered when evaluating inter-channel nonlinear interactions, SCA allows for an averaging over all relative positions within each nonlinear step providing higher accuracy estimates of the nonlinear interactions – relaxing the step-size requirements.

This paper is organized as follows. Section II presents the separate channels approach framework for WDM-SDM systems. Section III presents the WDM-SDM system to be used in this paper. Section IV presents and analyzes simulation results for the conventional DBP and for SCA-DBP over a wide range of *DMD* values and *LMC* strengths from the intermediate coupling regime to the strong coupling regime; extending our previous results in [39, 41, 47]. Section V draws the final conclusions.

II. Separate Channels Nonlinear Schrödinger Equation for SDM-WDM Systems

In order to find the nonlinear terms responsible for intermodal nonlinear interactions between a specific set of channels, the total electric field has to be written as a sum over M distinct modes, $N+1$ distinct frequencies, and 2 orthogonal polarizations. The total electric field vector in the frequency domain is given by:

$$\tilde{\mathbf{E}}(\mathbf{r},\omega) = \frac{1}{2}\tilde{E}_x(\mathbf{r},\omega)\hat{x} + \frac{1}{2}\tilde{E}_y(\mathbf{r},\omega)\hat{y} + c.c. =$$

$$\sum_{dsl}\left[\frac{1}{2}\frac{F_d(x,y)}{\sqrt{N_u}}\tilde{A}_{dsl}(z,\omega-\omega_v)\exp\left(-j\beta_{dsl}^{(0)}z\right)\hat{\imath} + c.c.\right] \quad (1)$$

where $d = \{1,\dots,M\}$ is the mode index, $s = \{-N/2,\dots,N/2\}$ is the frequency channel index (N even, without lack of generality), $l = \{1,2\}$ is the polarization index ($l = 1$ refers to x-polarization and $l = 2$ refers to y-polarization), $\mathbf{r}$ is the position vector in Cartesian coordinates (x, y, z), ω is the angular frequency, $\hat{l}$ is the unit linear polarization vector, j is the imaginary unit, $\sum_{dsl} = \sum_{d=1}^{M}\sum_{s=-N/2}^{N/2}\sum_{l=1}^{2}$, $F_d(x,y)$ is the transversal field distribution of mode d, $\tilde{A}_{dsl}(z,\omega-\omega_s)$ is the Fourier transform of the slowly varying wave envelope $A_{dsl}(z,t)$ (t is the time variable), $N_d = \iint|F_d(x,y)|^2 dxdy$ such that $F_d(x,y)/\sqrt{N_d}$ is the normalized electrical field distribution, $\beta_{dsl}^{(0)}$ is the value of the frequency dependent propagation constant $\beta_{dl}(\omega)$ at ω_s, and $c.c.$ stands for complex

conjugate. Note that in (1), $F_d(x,y)$ is assumed to vary negligibly with ω within the C-band [48]. $F_d(x,y)$ and $\beta_{dl}(\omega)$ are solutions of the eigenvalue equation [48].

The propagation of the total electric field is governed by the wave equation [48]:

$$\nabla^2\tilde{\mathbf{E}}(\mathbf{r},\omega) = -\omega^2\mu_0\varepsilon_{pr}(x,y)\tilde{\mathbf{E}}(\mathbf{r},\omega) - \omega^2\mu_0\tilde{\mathbf{P}}_{NL}(\mathbf{r},\omega) \quad (2)$$

where $\tilde{\mathbf{P}}_{NL}(\mathbf{r},\omega)$ is the Fourier transform of the nonlinear polarization $\mathbf{P}_{NL}(\mathbf{r},t)$ due to the third-order nonlinear silica susceptibility $\chi_{xxxx}^{(3)}$. Mode coupling can be included in (2) by replacing $\varepsilon_{pr}(x,y)$ with $\varepsilon(x,y) = \varepsilon_{pr}(x,y) + \Delta\varepsilon(x,y)$ where $\Delta\varepsilon$ denotes the random perturbation in each fiber section. Here we follow the model in [8], fluctuations of the fiber core-cladding boundary are introduced by dividing the fiber in multiple sections each with a random displacement of the core center position, such that: $\varepsilon(x,y) = \varepsilon_{pr}(x+\delta x, y+\delta y)$. This model has been proven accurate in matching the analytical predictions for the statistics of GDs in FMF links for all coupling regimes and over a wide range transmission lengths 10 m-to-10,000 km [8]. Please see Fig. 8 in [8] for insight into the shape of the fiber impulse response.

The wave equation (2) can be solved replacing (1), the eigenvalue equation, the Taylor series of $\beta_{dl}(\omega)$ around ω_s and applying the inverse Fourier transform. Afterwards, considering the slowly varying envelope approximation (in space and time) [48], selecting mode d by multiplying both sides by F_d^* and integrating over the x-y transverse plane, and selecting the terms oscillating at each specific frequency ω_s such that $\omega_p + \omega_q - \omega_r - \omega_s = 0$, a coupled nonlinear Schrödinger equation (CNLSE) can be written as:

$$\left(\partial_z + \mathcal{D} + \frac{\alpha_{dsl}}{2}\right)A_{dsl}$$

$$= -j\sum_{api}\sum_{bqj}\sum_{crk}\left[\begin{matrix}\xi_{ijkl}\gamma_{abcd}A_{api}A_{bqj}A_{crk}^*\\ \cdot e^{-j\Delta\beta_{api,bqj,crk,dsl}z}\end{matrix}\right] \quad (3)$$

$$-j\sum_{ai}A_{asi}C_{asi,dsl}e^{j\left(\beta_{dsl}^{(0)}-\beta_{asi}^{(0)}\right)z}$$

$$\mathcal{D} = \beta_{dsl}^{(1)}\partial_t - j\frac{\beta_{dsl}^{(2)}}{2}\partial_t^2 - \frac{\beta_{dsl}^{(3)}}{6}\partial_t^3 \quad (4)$$

$$\beta_{dsl}^{(m)} = \partial_\omega^m\beta_{dl}(\omega)|_{\omega=\omega_s} \quad (m = 1,2,\dots) \quad (5)$$

$$\xi_{ijkl} = \delta_{il}\delta_{jl}\delta_{kl} + \frac{2}{3}\delta_{il}\delta_{jl_\perp}\delta_{kl_\perp} + \frac{1}{3}\delta_{il_\perp}\delta_{jl_\perp}\delta_{kl} \quad (6)$$

$$\Delta\beta_{api,bqj,crk,dsl} = \beta_{api}^{(0)} + \beta_{bqj}^{(0)} - \beta_{crk}^{(0)} - \beta_{dsl}^{(0)} \quad (7)$$

$$\gamma_{abcd} = n_2\omega_s/c_0A_{abcd}^{eff} \quad (8)$$

$$C_{asi,dsl} = \frac{\omega_s^2\mu_0}{2\beta_{dsl}^{(0)}}\iint \Delta\varepsilon(x,y)\frac{F_aF_d^*}{\sqrt{N_aN_d}}dxdy \quad (9)$$

where (a, b, c, d) are mode indices, (p, q, r, s) are frequency indices, (i, j, k, l) are polarization indices, * stands for complex conjugate; $\mathcal{D}$ in (4) accounts for chromatic dispersion and DMD; $\beta_{dsl}^{(m)}$ in (5) is the value of the mth derivative of the frequency dependent propagation constant $\beta_{dl}(\omega)$ at ω_s; ξ_{ijkl} in (6) groups the independent polarization combinations using the Kronecker delta function δ_{il}; $\Delta\beta_{api,bqj,crk,dsl}$ in (7) is the

phase mismatch between waves api, bqj, crk and dsl; γ_{abcd} in (8) is the nonlinear coefficient between modes (a, b, c, d); A_{abcd}^{eff} in (8) is the inter-mode effective area (A^{eff}) between modes (a, b, c, d); n_2 in (8) is the Kerr coefficient, approximately equal to $2.6 \cdot 10^{-20}$ m²/W[48]; $C_{asi,dsl}$ in (9) is the LMC coefficient between mode d and mode a. The first term on the right-hand side of (3) is responsible for all the nonlinear effects taking place between the wave dsl and the all the other $2 \times M \times (N + 1)$ waves (including itself), this is, it includes all the terms responsible by: self-phase modulation (SPM), intra-mode XPM, IM-XPM, intra-mode FWM, and IM-FWM. The second term on right-hand side of (3) is responsible for the LMC.

The CNLSE (3) can be simplified considering the phase mismatch properties. Considering a common reference frequency ω_0, the terms in the RHS of (7) can be written as $\beta_{api}^{(0)} \cong \beta_{ai}(\omega_0) - \beta_{api}^{(1)}(\omega_0 - \omega_p)$, thereby:

$$
\begin{aligned}
&\Delta\beta_{api,bqj,crk,dsl} \\
&\cong \begin{pmatrix} \beta_{ai}(\omega_0) + \beta_{bj}(\omega_0) \\ -\beta_{ck}(\omega_0) - \beta_{dl}(\omega_0) \end{pmatrix} \\
&+ \begin{pmatrix} -\beta_{api}^{(1)} \cdot (\omega_0 - \omega_p) - \beta_{bqj}^{(1)} \cdot (\omega_0 - \omega_q) \\ +\beta_{crk}^{(1)} \cdot (\omega_0 - \omega_k) + \beta_{dsl}^{(1)} \cdot (\omega_0 - \omega_s) \end{pmatrix}
\end{aligned}
\tag{10}
$$

Assuming that $|\beta_{dl}(\omega_0)| \gg |\beta_{dsl}^{(1)} \cdot (\omega_0 - \omega_s)|$ for any dsl with ω_s and ω_0 in the C-band, phase mismatch (10) can only be made approximately zero if the terms in the first parenthesis in the RHS of (10) can be made approximately zero. Furthermore, assuming that even for pairs of degenerate linearly polarizer (LP) modes the effective index difference is not lower than $\sim 10^{-5}$ [49], the possible mode matching conditions are $(a = m, b = n, c = n, d = m)$ and $(a = n, b = m, c = n, d = m)$. Considering the abovementioned phase mismatch properties, the CNLSE are given by:

$$
\begin{aligned}
&\left(\partial_z + \mathcal{D} + \frac{\alpha_{msl}}{2} \right) A_{msl} \\
&= -j \begin{pmatrix} C_{SPM} + C_{XPM} + C_{FWM} \\ + C_{IM-XPM} + C_{IM-FWM} \end{pmatrix} \\
&\quad - j \sum_{ni} A_{nsi} C_{nsi,msl} e^{j(\beta_{msl}^{(0)} - \beta_{nsi}^{(0)})z}
\end{aligned}
\tag{11}
$$

$$
C_{SPM} = \gamma_{mmmm} |A_{msl}|^2 A_{msl}
\tag{12}
$$

$$
C_{XPM} = 2\gamma_{mmmm} \cdot \left(\sum_{p \neq s} |A_{mpl}|^2 + \frac{1}{3} \sum_p |A_{mpl_\perp}|^2 \right) A_{msl}
\tag{13}
$$

$$
C_{IM-XPM} = 2 \sum_{n \neq m} \sum_p \gamma_{mnnm} \left(|A_{npl}|^2 + \frac{1}{3} |A_{npl_\perp}|^2 \right) A_{msl}
\tag{14}
$$

$$
C_{FWM} = \sum_{pi} \sum_{qj} \sum_{rk \neq pi \wedge qj} \begin{pmatrix} \xi_{ijkl} \gamma_{mmmm} A_{mpi} A_{mqj} \\ \cdot A_{mrk}^* e^{-j\Delta\beta_{mpi,mqj,mrk,msl}z} \end{pmatrix}
\tag{15}
$$

$$
C_{IM-FWM} = \sum_{n \neq m} \sum_{pi} \sum_{qj} \sum_{rk \neq qj} \begin{pmatrix} \psi_{ijkl} \gamma_{mnnm} \\ \cdot A_{mpi} A_{nqj} A_{nrk}^* \\ \cdot e^{-j\Delta\beta_{mpi,nqj,nrk,msl}z} \end{pmatrix}
\tag{16}
$$

$$
\begin{aligned}
\psi_{ijkl} &= 2\delta_{il}\delta_{jl}\delta_{kl} + \frac{2}{3}\delta_{il}\delta_{jl_\perp}\delta_{kl_\perp} + \frac{2}{3}\delta_{il_\perp}\delta_{jl}\delta_{kl_\perp} \\
&\quad + \frac{2}{3}\delta_{il_\perp}\delta_{jl_\perp}\delta_{kl}
\end{aligned}
\tag{17}
$$

In the first term on the RHS of (11) the nonlinear contributions due to SPM (C_{SPM}) (12), intra-mode XPM (C_{XPM}) (13), intra-mode FWM (C_{FWM}) (14), IM-XPM (C_{IM-XPM}) (15) and IM-FWM (C_{IM-FWM}) (16) are identified. Finally, (11) can be solved using the SSFM modified for multimode propagation including LMC as in [14].

Focusing here on back-propagation, the LMC in (11) can be dismissed. Moreover, assuming negligible FWM terms, C_{FWM} and C_{IM-FWM} are nulled. For operation in the strong coupling regime, the nonlinear degeneracy factors and the nonlinear coefficients in (12-14) are analytically averaged over all possible occurrences of the LMC operator, considering that all modes are strongly linearly coupled. In this way, the nonlinear degeneracy factors and the nonlinear coefficients in (12-14) are replaced by a single value κ given by [12]:

$$
\kappa = \frac{4}{3} \frac{2M}{2M + 1} \left(\frac{1}{M^2} \sum_{u,v} \gamma_{uvvu} \right)
\tag{18}
$$

In deriving (18), it is assumed that spatial modes that are strongly coupled propagate with similar group delay (that is, *DMD* should not be higher than a few ps/km).

In the strong coupling regime C_{SPM}, C_{XPM}, C_{IM-XPM} became:

$$
C_{SPM} = \kappa |A_{msl}|^2 A_{msl}
\tag{19}
$$

$$
C_{XPM} = \kappa \sum_{p \neq s} \sum_i |A_{mpi}|^2 A_{msl}
\tag{20}
$$

$$
C_{IM-XPM} = \kappa \sum_{n \neq m} \sum_p \sum_i |A_{npi}|^2 A_{msl}
\tag{21}
$$

III. INTRA-MODE AND IM-XPM POST-COMPENSATION USING DIGITAL BACKWARD PROPAGATION

The above system of equations (11) is solved in the digital domain with the SSFM with the linear and nonlinear parts solved independently which is accurate over a sufficiently short distance. For the implementation of the DBP algorithm we use a constant step size h.

The linear step in (11) is solved in the frequency domain with a transfer function given by:

$$
\begin{aligned}
H_{msl}(\omega, h) = \exp &\left[j \left(\beta_{msl}^{(1)}(\omega - \omega_s) + \frac{\beta_{msl}^{(2)}}{2}(\omega - \omega_s)^2 \right. \right. \\
&\left. \left. + \frac{\beta_{msl}^{(3)}}{6}(\omega - \omega_s)^3 \right) h \right]
\end{aligned}
\tag{22}
$$

assuming that the spectral change induced by nonlinearity is

weak along the step length. The nonlinear step solution is conventionally given by:

$$E_{msl}(t, z + h) = E_{msl}(t, z)\exp\left[j\varphi_{SPM} + j\varphi_{XPM} + j\varphi_{IM-XPM}\right] \quad (23)$$

where φ_{IM-XPM}, the inter-mode XPM-induced phase modulation generated in the current split step, is conventionally obtained by:

$$\varphi_{IM-XPM}(t, z) = C_{IM-XPM}h \quad (24)$$

φ_{SPM} and φ_{XPM} are obtained in the same fashion. However, through spatial integration, just like for SMF systems [42], the IM-XPM-induced phase modulation can be expressed in the frequency domain as follows:

$$\varphi_{IM-XPM}(f, z)$$
$$= \sum_{n \neq m} \sum_{p} \sum_{i} \left[\kappa \frac{1 - \exp[-(\alpha - j2\pi f d_{npi,msl})h]}{\alpha - j2\pi f d_{npi,msl}} \cdot \right. \quad (25)$$
$$\left. \exp\left[(\alpha - j2\pi f d_{npi,msl})\frac{h}{2}\right] \cdot F\left\{\left|A_{npi}\left(t, z + \frac{h}{2}\right)\right|^2\right\}\right]$$

$$d_{npi,msl} = \beta_{n0i}^{(2)}(\omega_p - \omega_0) - \beta_{m0l}^{(2)}(\omega_s - \omega_0) + \left(\beta_{n0i}^{(1)} - \beta_{m0l}^{(1)}\right) \quad (26)$$

where $d_{npi,msl}$ is the walk-off between the channel p (at mode n polarization i) and channel s (at mode m polarization l), and F represents the Fourier transform. $\beta_{n0i}^{(2)}$ is the $\beta^{(2)}$ of mode n polarization i at ω_0. In contrast to (24), where only one value of the relative position between the channels npi and msl is taken into account, (25) is the result of an averaging over all relative positions within one split-step, which is the key idea of [42]. As a result, much larger step sizes are allowed. Note that (24) neglects the conversion of the induced phase modulation into intensity modulation which is a reasonable approach since the conversion within one split-step is weak [50].

The approach in (25), involving a frequency domain filter, requires an additional direct and inverse Fourier transform increasing the complexity per step. However, by factorizing the walk-off effect, the step size can be substantially increased in typical WDM-SDM scenarios, where the walk-off length is much shorter than both the nonlinear length and the intra-channel dispersion length. Therefore, significant savings in computation are anticipated.

In our implementation of the separate channels approach, after coherent detection, the channels were first digitally demultiplexed using brick wall filters following a down-sampling to $2 \times$ samples/symbol before DBP. In this case, the DBP nonlinear step is implemented using the filters calculated in accordance to (25), this is:
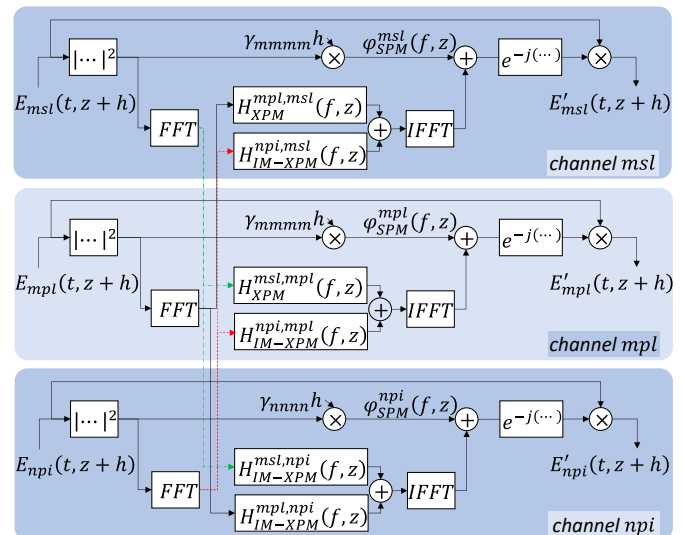

Fig. 1. Block diagram for the nonlinear operator implementation considering explicitly a sub-set of three channels.

$$H_{IM-XPM}^{npi,msl}(f, z) = \kappa \frac{1 - \exp[-(\alpha - j2\pi f d_{npi,msl})h]}{\alpha - j2\pi f d_{npi,msl}} \cdot \exp\left[(\alpha - j2\pi f d_{npi,msl})\frac{h}{2}\right] \quad (27)$$

For example, for a 19-channel system with 12 polarization modes we need $12 \times 19 \times (19-1) = 4104$ filters per step. Therefore, the implementation of this large number of filters requires practical efficiency. Fortunately, the filters in (27) can be pre-computed prior to running the DBP. Only two fast Fourier transforms (which are the most time-consuming operations of the calculation) per channel are required for the application of the filters in (27). Fig. 1 presents a block diagram for the nonlinear operator implementation. The phase modulation induced by each channel is accounted by applying the filters in (27) to the Fourier transform of the intensity of interfering channel (already calculated for the SPM step) – following the same structure proposed in [42]. The phase induced spectrums are then added in the frequency domain, Fourier transformed to the time-domain, and finally applied to the signal together with SPM induced phase.

IV. SIMULATION SETUP

In this section we describe the WDM-SDM transmission setup used to evaluate the SCA-DBP potential.

The simulation setup is shown in Fig. 2. A mode-division-multiplexing system using a FMF with 6 linearly polarized (LP) modes (LP$_{01}$, LP$_{02}$, LP$_{11a}$, LP$_{11b}$, LP$_{21a}$ and LP$_{21b}$) each with 2 orthogonal polarizations is considered. The fiber was optimized in [51] for low DMD; linear and nonlinear characteristics at 1550 nm are given in table I and II, respectively. Transmission simulations consider an optical super-channel with a varying number of WDM channels (per mode) modulated with 14 Gbaud polarization-multiplexed 16QAM, 15 GHz spaced; the line rate per channel is 672 Gbit/s. Together with the information data, a preamble is transmitted consisting of constant amplitude zero autocorrelation (CAZAC) sequences, used for time synchronization and channel estimation. Root
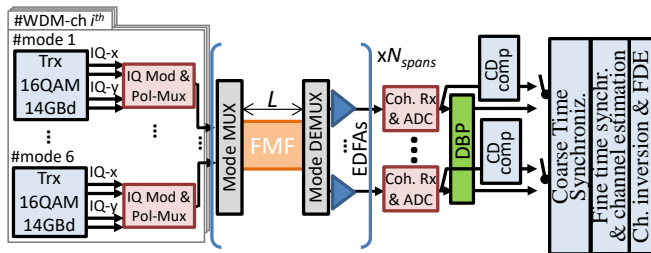
Fig. 2. Block diagram for system simulations using a fibre with 6 LP modes each with 2 orthogonal polarizations.

TABLE I. FIBRE LINEAR CHARACTERISTICS AT 1550NM.

u	LP01	LP02	LP11a	LP11b	LP21a	LP21b
$\beta_u^{(1)}$ [ps/km]	-0.29	-2.93	-0.66	-0.66	2.27	2.27
$\beta_u^{(2)}$ [ps²/km]	-28.28	-27.48	-28.25	-28.25	-27.86	-27.86
$\beta_u^{(3)}$ [ps³/km]	0.15	0.15	0.15	0.15	0.15	0.15
α_u [dB/km]	0.2	0.2	0.2	0.2	0.2	0.2

TABLE II. NONLINEAR COEFFICIENTS* (γ_{uv}) [W⁻¹/KM] AT 1550NM.

u $\quad$ v	LP01	LP02	LP11a	LP11b	LP21a	LP21b
LP01	0.73	0.36	0.36	0.36	0.18	0.18
LP02	0.36	0.36	0.18	0.18	0.18	0.18
LP11a	0.36	0.18	0.55	0.18	0.27	0.27
LP11b	0.36	0.18	0.18	0.55	0.27	0.27
LP21a	0.18	0.18	0.27	0.27	0.41	0.14
LP21b	0.18	0.18	0.27	0.27	0.14	0.41

*Note that $\gamma_{uvij} = \gamma_{uvii} = \gamma_{uv}$, the degeneracy factors are explicitly considered in (2), (3) and (4).

raised cosine filters with a roll-off factor of 0.001 is used for pulse shaping. Simulations considered 2^{16} symbols per polarization mode, the first 2^{12} were CAZAC symbols and the remaining were 16-QAM symbols mapped from a subset of a 2^{23}-1 PRBS [52]. The fiber attenuation is fully compensated using an array of 6 erbium doped fiber amplifiers, considering a noise figure of 4.5 dB and negligible mode dependent gain since the aim of this section is to assess the impact of *LMC* and *DMD* on the accuracy of the different solution methods. Similarly, the mode multiplexer (MUX) and de-multiplexer (DEMUX) were assumed to be ideal for the same reasons. After homodyne detection, the baseband electrical signals are sampled at $2 \times N_{ch}$ samples/symbol (where N_{ch} stands for the number transmission channels per mode), yielding 12 digital signals (2 polarizations times 6 modes).

Afterwards, the coherently received signals are either (i) compensated for chromatic dispersion in the frequency domain using the values in the Table I or (ii) DBP compensated for chromatic dispersion and nonlinear distortion [53, 54] using a "virtual" fibre with characteristics of opposite-sign values of those in the Table I and II, except that no mode coupling or differential mode delay given the analytical averaging of the nonlinear operator in equation (18). Two DBP methods were followed: a conventional full bandwidth back propagation (as in [41]) and the separate channels approach discussed in section III. In all cases, *LMC* and (residual) *DMD* were subsequently compensated using data-aided channel estimation and equalization, as shown in Fig. 3. Coarse time synchronization is performed using the Schmidl & Cox autocorrelation metric. Subsequently, fine-time synchronization and channel impulse response (CIR) estimation are performed by cross-correlating with the training CAZAC sequences. The 12×12 CIR estimations are converted into the frequency domain. The MIMO frequency domain equalizer is calculated by inverting

the estimated channel matrix, and, finally, the signal-to-noise-ratio of the channel of interest is estimated [55].

The figure of merit in the following is the *minimum* signal-to-noise-ratio (SNR) among the 12 polarization modes guided of the center wavelength channel. The SNR is evaluated as [55] the ratio between the variance of the transmitted symbols $E[|X|^2]$ and the variance of the noise $E[|X - Y|^2]$, X and Y represent the received symbols, respectively. Note that, as explained in [55] Sec. V-B treating samples from a nonlinear channel (the case in this paper) as additive white Gaussian noise (AWGN) samples gives a lower bound on the performance and this is what the presented results indicate. For this reason the term effective SNR should be understood when refering to SNR in the following. Finally, system performance simulations consider spans of 50 km, a relatively short length that allows for larger a optical signal-to-noise-ratio while minimizing the total energy requirement. Note that the optimum length to minimize the total energy requirement for amplified systems with a fibre loss of 0.2 dB/km is actually 35 km [56].

DBP performance is known to be strongly depend on the effective number of bits (ENoB) of the analog-to-digital convertors in the receiver front-end [57]. Therefore, we consider state-of-the-art analog-to-digital converters with an effective number of bits equal to 6.5 bits.

V. TRANSMISSION MODELS COMPARISON

This section compares the separate channels approach discussed in section III for DBP with a conventional full bandwidth DBP approach analyzed in [41]. Forward transmission simulation considers a symmetric implementation of the SSFM with an adaptable step size chosen by bounding the local error to be smaller than 10^{-5} (smaller values led to negligible change). Backward propagation is done in all cases considering a fix-step size. Simulations consider 19 channels per mode over 7 spans, for a wide range of *DMD* values (10 to 160 ps/km), and *LMC strengths* (-30dB/m to 0dB/m) – denoted as *XT*, see [8] for definition.

Fig. 3 shows the *SNR* as a function of the launch power for linear equalization, conventional full bandwidth DBP and SCA-
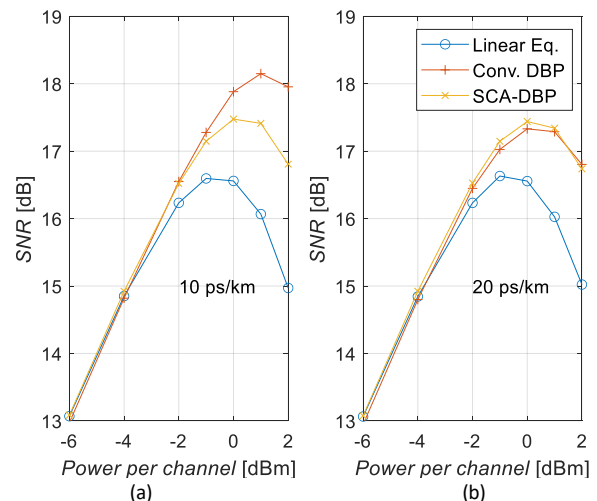

Fig. 3. *SNR* as a function of channel power for linear equalization, conventional DBP and SCA-DBP, with a DBP step size of 350 m, for a *XT* of 0 dB/m and a *DMD* of: (a) 10 ps/km and (b) 20ps/km. Results averaged over 10 repetitions.
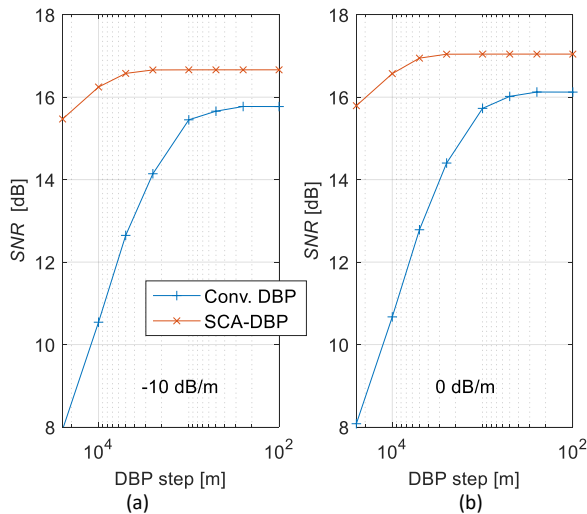
Fig. 4. *SNR* with conventional DBP and SCA-DBP as a function of the DBP step for high *DMD* (160 ps/km) and a *XT* of: (a) -10 dB/m and (b) 0 dB/m. The launch power is 0dBm in all cases. Results averaged over 10 repetitions.

DBP. The results were obtained with a DBP step size of 350 m for a *XT* of 0 dB/m and a *DMD* of: (a) 10 ps/km and (b) 20 ps/km. As expected from previous works, for very low *DMD* and extremely strong *XT*, conventional DBP offers the most gain. But, as *DMD* increases, the performance of conventional DBP can degrade quickly, as seen in Fig. 3.

Fig. 4 compares the step size requirements for nonlinear compensation using conventional DBP and SCA-DBP at 0 dBm/channel for high *DMD* (160ps/km) and two *XT* values: (a) -10dB/m and (b) 0dB/m. For both *XT* values we can see that the step required for a given technique to achieve quasi-optimum performance is 250 m for conventional DBP and 2500 m for SCA-DBP. The step requirement for SCA-DBP is 10-times smaller. We can also see that in both cases SCA-DBP outperforms conventional DBP, an improvement of 1 dB at maximum nonlinear compensation performance (this is, for an arbitrarily small step. In other words, SCA-DBP outperforms conventional DBP by 1 dB using a 10-times larger DBP step.

Fig. 5 shows *SNR gain* over linear equalization as a function of *XT* with varying *DMD*, considering: (a) conventional DBP with a step of 250 m and (b) SCA-DBP with a step of 2500 m. The *SNR gain* is calculated for the optimum launch power of each equalization technique at each (*XT*, *DMD*) combination. Note that a double tick line is used to highlight the range of *DMD* and *XT* values leading to a *GD spread* equal or higher than the lowest value experimentally reported to date, 2.5ps/√km [30]. The figure shows that for *DMD* ≥ 20 ps/km, SCA-DBP outperforms conventional DBP for any *XT* value, the performance advantage ranges from 0.3 to 0.8 dB over a range of *DMD* and *XT* values compatible with the CC-MCF presented in [30]. For smaller *DMD* values and extremely high *XT* values (≥-10 dB/m), SCA-DBP is out-performed by conventional DBP. In this latter case, DMD and LMC have not fully suppressed FWM interactions and conventional DBP succeeds in partially accounting for those – this regime resembles that of conventional SMF links.

Finally, one can conclude that for significant *XT* and *DMD* values (≥-30 dB/m and ≥20 ps/km, respectively) the SCA-DBP provides a substantial *SNR improvement* (~0.5 dB) on top of what conventional DBP achieves with much lower complexity
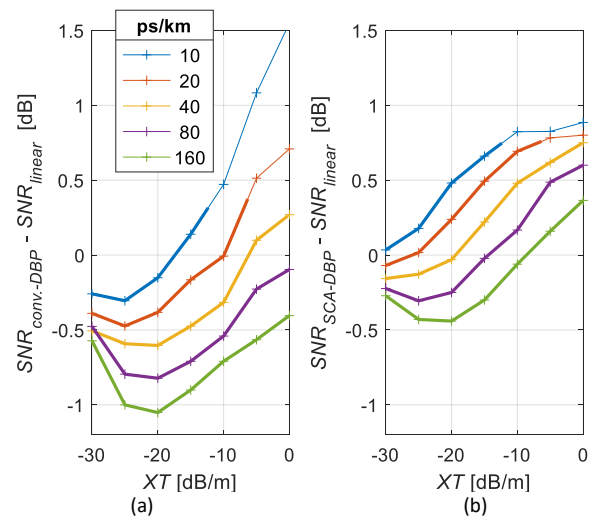

Fig. 5. *SNR gain* over linear equalization as a function *XT* with varying *DMD* from 10-to-160 ps/km, for: (a) conventional DBP with a step of 250m and (b) SCA-DBP with a step of 2500m. Note that for each equalization technique the respective optimum launch power is used. Results averaged over 10 repetitions.

(~10-times). For extremely high *XT* and low *DMD*, (0 dB/m and <20 ps/km, respectively), conventional DBP may perform better at the expense of additional complexity, this is a much smaller step size (~10-times).

VI. CONCLUSION

This work shows that even for the complex spatial multiplexed systems under challenging LMC and DMD conditions there is significant potential for performance improvement using DBP. We have shown that a separate channels approach can be used to improve DBP performance, in particular, for fibers with significant *XT* and *DMD* (≥-30 dB/m and ≥20 ps/km, respectively). Importantly, such an improved technique has been shown to reduce the DBP step requirements by a factor of 10 while improving maximum-effort performance by as much as 0.8 dB. The technique investigated in this paper is an important step towards the development of digital nonlinear compensation for spatial multiplexed systems.

REFERENCES

[1] D. J. Richardson, J. M. Fini, and L. E. Nelson, "Space-division multiplexing in optical fibres," *Nature Photonics,* Review Article vol. 7, p. 354, 04/29/online 2013.

[2] P. J. Winzer and D. T. Neilson, "From Scaling Disparities to Integrated Parallelism: A Decathlon for a Decade," *Journal of Lightwave Technology,* vol. 35, no. 5, pp. 1099-1115, 2017.

[3] D. M. Marom *et al.*, "Survey of photonic switching architectures and technologies in support of spatially and spectrally flexible optical networking [invited]," *IEEE/OSA Journal of Optical Communications and Networking,* vol. 9, no. 1, pp. 1-26, 2017.

[4] F. Ferreira, P. Monteiro, and H. Silva, "Semi-analytical model for linear modal coupling in few-mode fiber transmission," in *2012 14th*

International Conference on Transparent Optical Networks (ICTON), 2012: IEEE.

[5] K.-P. Ho and J. M. Kahn, "Linear Propagation Effects in Mode-Division Multiplexing Systems," *Journal of Lightwave Technology,* vol. 32, no. 4, pp. 614-628, 2014.

[6] A. Mecozzi, C. Antonelli, and M. Shtaif, "Intensity impulse response of SDM links," *Opt Express,* vol. 23, no. 5, pp. 5738-43, Mar 9 2015.

[7] C. Antonelli, A. Mecozzi, and M. Shtaif, "The delay spread in fibers for SDM transmission: dependence on fiber parameters and perturbations," *Opt Express,* vol. 23, no. 3, pp. 2196-202, Feb 9 2015.

[8] F. M. Ferreira, C. S. Costa, S. Sygletos, and A. D. Ellis, "Semi-Analytical Modelling of Linear Mode Coupling in Few-Mode Fibers," *Journal of Lightwave Technology,* vol. 35, no. 18, pp. 4011-4022, 2017.

[9] J. Vuong, P. Ramantanis, A. Seck, D. Bendimerad, and Y. Frignac, "Understanding discrete linear mode coupling in few-mode fiber transmission systems," in *2011 37th European Conference and Exhibition on Optical Communication*, 2011, pp. 1-3.

[10] B. Inan *et al.*, "DSP complexity of mode-division multiplexed receivers," *Opt. Express,* vol. 20, no. 10, p. 10859, 2012 2012.

[11] A. Mecozzi, C. Antonelli, and M. Shtaif, "Coupled Manakov equations in multimode fibers with strongly coupled groups of modes," *Optics Express,* vol. 20, no. 21, pp. 23436-23441, 2012/10/08 2012.

[12] A. Mecozzi, C. Antonelli, and M. Shtaif, "Nonlinear propagation in multi-mode fibers in the strong coupling regime," *Optics Express,* vol. 20, no. 11, pp. 11673-11678, 2012/05/21 2012.

[13] S. Mumtaz, R.-J. Essiambre, and G. P. Agrawal, "Nonlinear Propagation in Multimode and Multicore Fibers: Generalization of the Manakov Equations," *Journal of Lightwave Technology,* vol. 31, no. 3, pp. 398-406, 2013.

[14] F. Ferreira, S. Jansen, P. Monteiro, and H. Silva, "Nonlinear semi-analytical model for simulation of few-mode fiber transmission," *IEEE Photonics Technology Letters,* vol. 24, no. 4, pp. 240--242, 2 2012.

[15] C. Koebele, M. Salsi, G. Charlet, and S. Bigo, "Nonlinear Effects in Mode-Division-Multiplexed Transmission Over Few-Mode Optical Fiber," *IEEE Photonics Technology Letters,* vol. 23, no. 18, pp. 1316-1318, 2011.

[16] F. Poletti and P. Horak, "Description of ultrashort pulse propagation in multimode optical fibers," *Journal of the Optical Society of America B,* vol. 25, no. 10, pp. 1645-1654, 2008/10/01 2008.

[17] A. Lobato, J. Rabe, F. Ferreira, M. Kuschnerov, B. Spinnler, and B. Lankl, "Near-ML detection for MDL-impaired few-mode fiber transmission," *Optics Express,* vol. 23, no. 8, pp. 9589--9601, 4 2015.

[18] K.-P. Ho and J. M. Kahn, "Mode-dependent loss and gain: statistics and effect on mode-division multiplexing," *Optics Express,* vol. 19, no. 17, pp. 16612-16635, 2011/08/15 2011.

[19] C. Antonelli, A. Mecozzi, M. Shtaif, and P. J. Winzer, "Modeling and performance metrics of MIMO-SDM systems with different amplification schemes in the presence of mode-dependent loss," *Optics Express,* vol. 23, no. 3, pp. 2203-2219, 2015/02/09 2015.

[20] A. Lobato *et al.*, "Impact of mode coupling on the mode-dependent loss tolerance in few-mode fiber transmission," *Opt. Express,* vol. 20, no. 28, p. 29776, 2012 2012.

[21] F. M. Ferreira, C. S. Costa, S. Sygletos, and A. D. Ellis, "Nonlinear Performance of Few-Mode Fiber Links With Intermediate Coupling," *Journal of Lightwave Technology,* vol. 37, no. 3, pp. 989-999, 2019/02/01 2019.

[22] F. Ferreira, N. Mac Suibhne, C. Sánchez, S. Sygletos, and A. D. Ellis, "Advantages of Strong Mode Coupling for Suppression of Nonlinear Distortion in Few-Mode Fibers," in *Optical Fiber Communication Conference*, Anaheim, California, 2016, p. Tu2E.3: Optical Society of America.

[23] L. An, A. A. Amin, C. Xi, and W. Shieh, "Reception of mode and polarization multiplexed 107-Gb/s CO-OFDM signal over a two-mode fiber," in *2011 Optical Fiber Communication Conference and Exposition and the National Fiber Optic Engineers Conference*, 2011, pp. 1-3.

[24] L. Gruner-Nielsen *et al.*, "Few Mode Transmission Fiber With Low DGD, Low Mode Coupling, and Low Loss," *Journal of Lightwave Technology,* vol. 30, no. 23, pp. 3693-3698, 2012.

[25] R. Ryf *et al.*, "Mode-Division Multiplexing Over 96 km of Few-Mode Fiber Using Coherent 6$\,\times\,$6 MIMO Processing," *Journal of Lightwave Technology,* vol. 30, no. 4, pp. 521-531, 2012.

[26] R. Ryf *et al.*, "Space-Division Multiplexed Transmission over 4200 km 3-Core Microstructured Fiber," in *National Fiber Optic Engineers Conference*, Los Angeles, California, 2012, p. PDP5C.2: Optical Society of America.

[27] T. Sakamoto, T. Mori, T. Yamamoto, and S. Tomita, "Differential Mode Delay Managed Transmission Line for WDM-MIMO System Using Multi-Step Index Fiber," *Journal of Lightwave Technology,* vol. 30, no. 17, pp. 2783-2787, 2012.

[28] T. Mori, T. Sakamoto, M. Wada, T. Yamamoto, and F. Yamamoto, "Low DMD four LP mode transmission fiber for wide-band WDM-MIMO system," in *2013 Optical Fiber Communication Conference and Exposition and the National Fiber Optic Engineers Conference (OFC/NFOEC)*, 2013, pp. 1-3.

[29] T. Hayashi, Y. Tamura, T. Hasegawa, and T. Taru, "Record-Low Spatial Mode Dispersion and Ultra-Low Loss Coupled Multi-Core Fiber for Ultra-Long-Haul Transmission," *Journal of Lightwave Technology,* vol. 35, no. 3, pp. 450-457, 2017.

[30] T. Hayashi *et al.*, "Field-Deployed Multi-Core Fiber Testbed," in *2019 24th OptoElectronics and Communications Conference (OECC) and 2019 International Conference on Photonics in Switching and Computing (PSC)*, 2019, pp. 1-3.

[31] C. S. Costa, F. M. Ferreira, N. M. Suibhne, S. Sygletos, and A. D. Ellis, "Receiver Memory Requirement in Mode Delay Compensated Few-Mode Fibre Spans with Intermediate Coupling," in *ECOC 2016; 42nd European Conference on Optical Communication*, 2016, pp. 1-3.

[32] S. Ö. Arik, D. Askarov, and J. M. Kahn, "Effect of Mode Coupling on Signal Processing Complexity in Mode-Division Multiplexing," *Journal of Lightwave Technology,* vol. 31, no. 3, pp. 423-431, 2013.

[33] R. Ryf *et al.*, "Long-Distance Transmission over Coupled-Core Multicore Fiber," in *ECOC 2016 - Post Deadline Paper; 42nd European Conference on Optical Communication*, 2016, pp. 1-3.

[34] F. Ferreira, C. Sanchez, N. Suibhne, S. Sygletos, and A. Ellis, "Nonlinear Transmission Performance in Delay-Managed Few-Mode Fiber Links with Intermediate Coupling," in *Optical Fiber Communication Conference*, Los Angeles, California, 2017, p. Th2A.53: Optical Society of America.

[35] G. Rademacher *et al.*, "Long-Haul Transmission over Few-Mode Fibers with Space-Division Multiplexing," *Journal of Lightwave Technology,* vol. PP, no. 99, pp. 1-1, 2017.

[36] G. Rademacher *et al.*, "Wideband Intermodal Nonlinear Signal Processing With a Highly Nonlinear Few-Mode Fiber," *IEEE Journal of Selected Topics in Quantum Electronics,* vol. 26, no. 4, pp. 1-7, 2020.

[37] G. Rademacher *et al.*, "Investigation of Intermodal Nonlinear Signal Distortions in Few-Mode Fiber Transmission," *Journal of Lightwave Technology,* vol. 37, no. 4, pp. 1273-1279, 2019/02/15 2019.

[38] R. S. Luís, B. J. Puttnam, G. Rademacher, Y. Awaji, H. Furukawa, and N. Wada, "Digital Back Propagation in Long-Haul, MIMO-Supported, Multicore Fiber Transmission," *IEEE Photonics Technology Letters,* vol. 32, no. 12, pp. 730-732, 2020.

[39] F. M. Ferreira, C. S. Costa, S. Sygletos, and A. D. Ellis, "Overcoming degradation in spatial multiplexing systems with stochastic nonlinear impairments," *Scientific Reports,* vol. 8, no. 1, p. 17539, 2018/12/03 2018.

[40] D. J. Elson, D. Semrau, H. Takahashi, and T. Tsuritani, "Analytical Model for Transmission Performance of Single Mode Multicore Fibre with Nonlinearity Compensation," in *2019 24th OptoElectronics and Communications Conference (OECC) and 2019 International Conference on Photonics in Switching and Computing (PSC)*, 2019, pp. 1-3.

[41] F. M. Ferreira, S. Sygletos, E. Sillekens, R. Killey, A. D. Ellis, and N. J. Doran, "On the Performance of Digital Back Propagation in Spatial Multiplexing Systems," *Journal of Lightwave Technology,* vol. 38, no. 10, pp. 2790-2798, 2020.

[42] J. Leibrich and W. Rosenkranz, "Efficient numerical simulation of multichannel WDM transmission systems limited by XPM," *IEEE Photonics Technology Letters,* vol. 15, no. 3, pp. 395-397, 2003.

[43] E. Mateo, F. Yaman, and G. Li, "Efficient compensation of inter-channel nonlinear effects via digital backward propagation in WDM optical transmission," *Optics express,* vol. 18, pp. 15144-54, 07/05 2010.

[44] C. Häger and H. D. Pfister, "Wideband Time-Domain Digital Backpropagation via Subband Processing and Deep Learning," in *2018 European Conference on Optical Communication (ECOC)*, 2018, pp. 1-3.

[45] G. Liga, T. Xu, A. Alvarado, R. I. Killey, and P. Bayvel, "On the performance of multichannel digital backpropagation in high-capacity long-haul optical transmission," *Optics Express,* vol. 22, no. 24, pp. 30053-30062, 2014/12/01 2014.

[46] C. Antonelli, M. Shtaif, and A. Mecozzi, "Modeling of Nonlinear Propagation in Space-Division Multiplexed Fiber-Optic Transmission," *Journal of Lightwave Technology,* vol. 34, no. 1, pp. 36-54, 2016.

[47] F. M. Ferreira, "Linear and Nonlinear Features of Few-mode Fibers with Partial Coupling among Groups of Quasi-degenerate Modes," in *Optical Fiber Communication Conference (OFC) 2020*, San Diego, California, 2020, p. M3B.4: Optical Society of America.

[48] G. P. Agrawal, "Chapter 6 - Polarization Effects," in *Nonlinear Fiber Optics (Fifth Edition)*Boston: Academic Press, 2013, pp. 193-244.

[49] K.-P. Ho and J. M. Kahn, "Statistics of Group Delays in Multimode Fiber With Strong Mode Coupling," *Journal of Lightwave Technology,* vol. 29, no. 21, pp. 3119-3128, 2011.

[50] A. V. T. Cartaxo, "Cross-phase modulation in intensity modulation-direct detection WDM systems with multiple optical amplifiers and dispersion compensators," *Journal of Lightwave Technology,* vol. 17, no. 2, pp. 178-190, 1999.

[51] F. Ferreira, D. Fonseca, and H. J. A. Silva, "Design of few-mode fibers with M-modes and low differential mode delay," *Journal of Lightwave Technology,* vol. 32, no. 3, pp. 353--360, 2 2014.

[52] *O.150 – Series O: Specifications of measuring equipment*, 1996.

[53] E. Mateo, L. Zhu, and G. Li, "Impact of XPM and FWM on the digital implementation of impairment compensation for WDM transmission using backward propagation," *Optics Express,* vol. 16, no. 20, pp. 16124-16137, 2008/09/29 2008.

[54] E. Ip and J. M. Kahn, "Compensation of Dispersion and Nonlinear Impairments Using Digital Backpropagation," *Journal of Lightwave Technology,* vol. 26, no. 20, pp. 3416-3425, 2008.

[55] A. Alvarado, T. Fehenberger, B. Chen, and F. M. J. Willems, "Achievable Information Rates for Fiber Optics: Applications and Computations," *Journal of Lightwave Technology,* vol. 36, no. 2, pp. 424-439, 2018.

[56] N. J. Doran and A. D. Ellis, "Minimising total energy requirements in amplified links by optimising amplifier spacing," *Optics Express,* vol. 22, no. 16, pp. 19810-19817, 2014/08/11 2014.

[57] L. Galdino *et al.*, "On the limits of digital back-propagation in the presence of transceiver noise," *Optics Express,* vol. 25, no. 4, pp. 4564-4578, 2017/02/20 2017.